

## Muon-spin-spectroscopy study of the penetration depth of FeTe<sub>0.5</sub>Se<sub>0.5</sub>

P. K. Biswas,<sup>1</sup> G. Balakrishnan,<sup>1</sup> D. M. Paul,<sup>1</sup> C. V. Tomy,<sup>1,\*</sup> M. R. Lees,<sup>1,†</sup> and A. D. Hillier<sup>2</sup>

<sup>1</sup>Physics Department, University of Warwick, Coventry CV4 7AL, United Kingdom

<sup>2</sup>ISIS Facility, Rutherford Appleton Laboratory, Chilton, Oxfordshire OX11 0QX, United Kingdom

(Received 15 September 2009; revised manuscript received 11 March 2010; published 31 March 2010)

Muon-spin-spectroscopy measurements have been used to study the superconducting state of FeTe<sub>0.5</sub>Se<sub>0.5</sub>. The temperature dependence of the in-plane magnetic penetration depth,  $\lambda_{ab}(T)$ , is found to be compatible with either a two-gap  $s+s$ -wave or an anisotropic  $s$ -wave model. The value for  $\lambda_{ab}(T)$  at  $T=0$  K is estimated to be  $\lambda_{ab}(0)=534(2)$  nm.

DOI: 10.1103/PhysRevB.81.092510

PACS number(s): 74.70.Ad, 74.25.Ha, 76.75.+i

The discovery of superconductivity at high temperature in iron-based materials was a real surprise and has generated tremendous interest.<sup>1–3</sup> Iron selenium has recently been reported to be superconducting with a  $T_c$  of 8.0 K at ambient pressure<sup>4</sup> and 37 K at 7 GPa.<sup>5</sup> The substitution of tellurium on the selenium site increases  $T_c$  to maximum of 14.5 K at ambient pressure.<sup>6,7</sup> Magnetization and resistivity measurements indicate a lower critical field at  $T=0$  K,  $\mu_0 H_{c1}(0)$ , of between 1 and 8 mT and an upper critical field,  $\mu_0 H_{c2}(0)$ , of 40–60 T for the FeTe<sub>1-x</sub>Se<sub>x</sub> ( $0.25 \leq x \leq 0.5$ ) system.<sup>8–10</sup> Measurements on single crystals indicate that the superconducting properties of this material are anisotropic.<sup>9,10</sup>

Muon-spin rotation/relaxation, ( $\mu$ SR), a probe that is sensitive to the local-field distribution within a material, has often been used to measure the value and temperature dependence of the London magnetic penetration depth,  $\lambda$ , in the vortex state of type-II superconductors.<sup>11,12</sup>  $\lambda^2(T)$  is in turn proportional to  $n_s(T)$ , where  $n_s$  is the density of superconducting carriers. The temperature and field dependence of  $n_s$  can provide information on the nature of the superconducting gap.

Here we report a  $\mu$ SR study of FeTe<sub>0.5</sub>Se<sub>0.5</sub>. We show that the temperature dependence of  $\lambda$  can be equally well described using either a two-gap  $s+s$ -wave or an anisotropic  $s$ -wave model. We obtain an in-plane magnetic penetration depth  $\lambda_{ab}(0)=534(2)$  nm. We compare these results with published data for the FeTe<sub>1-x</sub>Se<sub>x</sub> ( $0.25 \leq x \leq 1.0$ ) system.

A polycrystalline sample of FeTe<sub>0.5</sub>Se<sub>0.5</sub> was synthesized in a two-step process from high-purity iron granules (99.999%), selenium shot (99.997%), and tellurium powder (99.999%). First, the appropriate stoichiometric mixture of elements were sealed in an evacuated carbon coated quartz tube ( $10^{-6}$  mbar) and heated at a rate of 100 °C/h to 650 °C, held at this temperature for 48 h, and then cooled to room temperature at 50 °C/h. The sample was then heated at a rate of 180 °C/h to 970 °C for 24 h and cooled to room temperature at 3 °C/h. Since the quartz tube often cracked during this cooling, the tube was sealed into a second quartz tube at a high vacuum before the second heating process.

X-ray diffraction measurements show the sample has a tetragonal PbO type structure (space group  $P4/nmm$ ) with  $a=b=0.3798(8)$  nm and  $c=0.6042(12)$  nm. The x-ray pattern showed that the sample also contained a quantity (<2%) of the hexagonal-NiAs phase of FeTe<sub>0.5</sub>Se<sub>0.5</sub> and some Fe<sub>3</sub>O<sub>4</sub> (~1%). Magnetization ( $M$ ) versus temperature ( $T$ ) measurements carried out in a Quantum Design MPMS

magnetometer reveal the sample has a transition temperature,  $T_c$ , of 14.4 K [see Fig. 1(a)]. The zero-field (ZF)-cooled dc susceptibility approaches a value of  $-1$  while the field-cooled signal is  $10^{-3}$  indicating strong pinning in the sample. Magnetization versus applied magnetic field loops collected in the normal state at 20, 150, and 350 K [see Fig. 1(b)] show that the normal-state signal is nearly temperature independent and has a response made up of contributions typical of a soft ferromagnet and a Pauli paramagnet. This is consistent with the presence in the sample of a small amount of Fe<sub>3</sub>O<sub>4</sub>. Using the published value for the saturation magnetization of Fe<sub>3</sub>O<sub>4</sub> (Ref. 13) we estimate this fraction to be ~0.5% of the

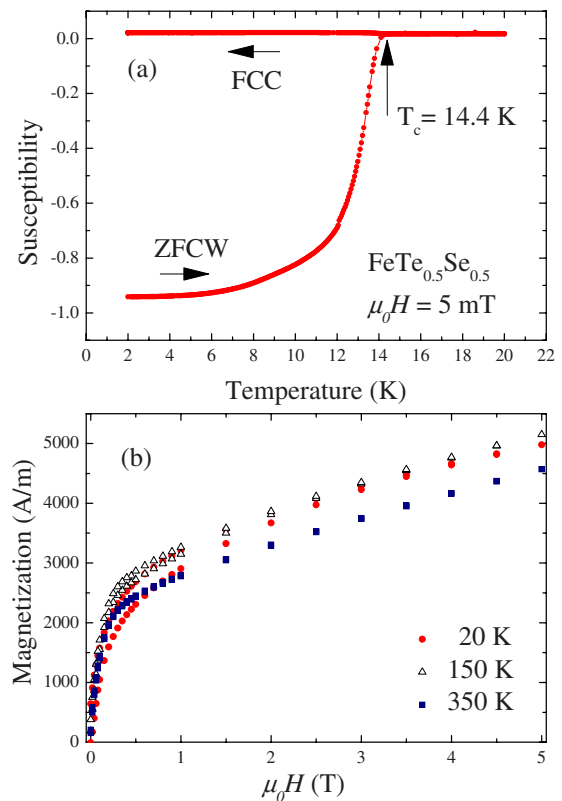


FIG. 1. (Color online) (a) Temperature dependence of the magnetic susceptibility of FeTe<sub>0.5</sub>Se<sub>0.5</sub> measured using zero-field-cooled warming and field-cooled cooling protocols. The diamagnetic susceptibility corresponds to complete diamagnetic screening with a  $T_c$  onset of 14.4 K. (b) Magnetization versus applied field curves for FeTe<sub>0.5</sub>Se<sub>0.5</sub> collected above  $T_c$  at 20, 150, and 350 K.

sample by mass<sup>14</sup> in agreement with our x-ray diffraction measurements.

The  $\mu$ SR measurements were performed using the MuSR spectrometer at ISIS. A pulse of muons is produced every 20 ms and has a full width at half maximum of  $\sim 70$  ns. The muons are implanted into the sample and decay with half life,  $\tau_\mu$ , of  $2.2 \mu\text{s}$  into positrons, which are emitted preferentially in the direction of the muon-spin axis. For a longitudinal-field measurement these positrons are detected and time stamped in the detectors which are positioned before ( $F$ ) and after ( $B$ ) sample. The positron counts  $N_{F,B}(t)$  have the functional form

$$N_{F,B}(t) = N_{F,B}(0) \exp\left(\frac{-t}{\tau_\mu}\right) [1 \pm G_Z(t)], \quad (1)$$

where  $G_Z(t)$  is the longitudinal relaxation function.  $G_Z(t)$  is determined using

$$\frac{N_F(t) - \alpha N_B(t)}{N_F(t) + \alpha N_B(t)}, \quad (2)$$

where  $\alpha$  is a calibration constant which is determined by applying a transverse field (TF) of 20 mT. Measurements were also carried out in TF mode in magnetic fields of up to 60 mT. Each detector is normalized for the muon decay and rotated into two components at  $90^\circ$  to one another.

The powder sample ( $30 \times 30 \text{ mm}^2$  and 1 mm thick) was mixed with GE varnish and mounted on a pure Ag plate. For measurements down to 1.2 K the sample was placed in a conventional Oxford Instruments cryostat. Data were also collected between 0.3 and 1 K in an Oxford Instruments He-3 cryostat. For the measurements in TF mode in the conventional cryostat, hematite slabs were positioned immediately behind the sample. For measurements in the He-3 cryostat these hematite slabs were removed to ensure good thermal contact between the sample and the cold stage of the cryostat leading to an increased background in the data collected. For all the data collected in a magnetic field presented in this paper, the sample was field cooled to base temperature and the data collected while warming the sample in a field. A set of data collected at 1.2 K in an applied magnetic field,  $\mu_0 H = 40$  mT after the sample was zero field cooled produced no usable signal due to the very strong pinning present in the sample.

ZF  $\mu$ SR data (see Fig. 2) can be fitted using

$$G_Z(t) = A_0 \exp(-\Lambda t), \quad (3)$$

where  $A_0$  is the initial asymmetry, with a small nearly  $T$  independent relaxation rate,  $\Lambda$ , of  $0.19 \mu\text{s}^{-1}$  between 20 and 1.2 K. The application of a small longitudinal magnetic field is sufficient to decouple the muon spin from the internal magnetic field. In line with the observations of Khasanov *et al.*<sup>15</sup> this suggests that the depolarization is caused by weak, static magnetic fields, that are present in the sample both above and below  $T_c$ . The most likely source of this field is dilute, randomly oriented magnetic moments associated with the  $\text{Fe}_3\text{O}_4$  impurity phase.

Figure 3 shows the TF- $\mu$ SR precession signals above and below  $T_c$ . In the normal state, the oscillation shows a small

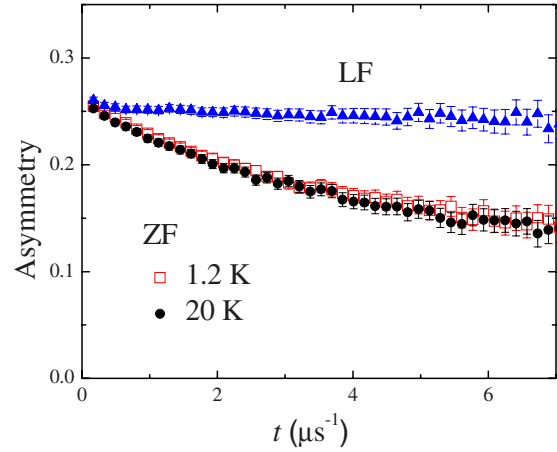


FIG. 2. (Color online) Zero-field ( $T=20$  and  $1.2$  K) and longitudinal-field ( $T=20$  K and  $\mu_0 H=30$  mT)  $\mu$ SR time spectra for a sample of  $\text{FeTe}_{0.5}\text{Se}_{0.5}$ .

relaxation. Below  $T_c$ , the relaxation rate increases due to the inhomogeneous field distribution of the flux-line lattice. Previous measurements on polycrystalline samples of superconducting materials have shown that the internal field distributions can be modeled using a sinusoidally oscillating function with a Gaussian component

$$G_X(t) = A_0 \exp(-\Lambda t) \exp(-\sigma^2 t^2) \cos(\omega t + \varphi), \quad (4)$$

where  $\omega$  is the muon precession frequency and  $\varphi$  is the phase offset.  $\sigma$  is the Gaussian relaxation rate given by  $\sigma = (\sigma_{sc}^2)$

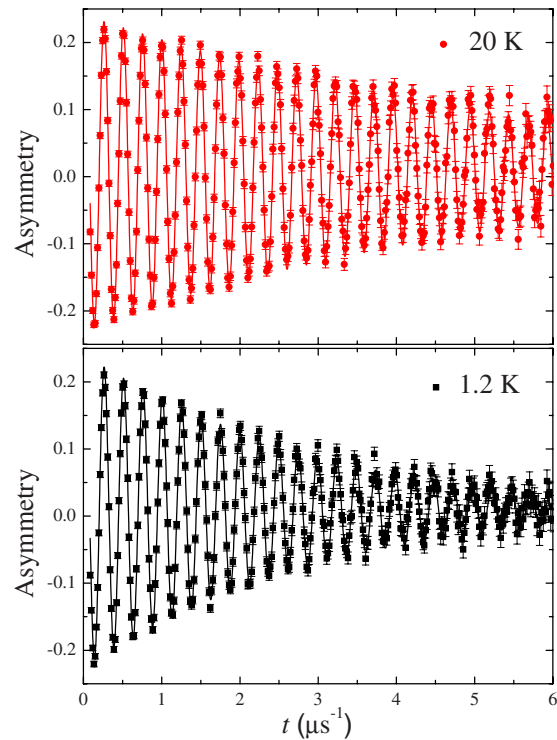


FIG. 3. (Color online) One component of the transverse-field muon-time spectra for  $\text{FeTe}_{0.5}\text{Se}_{0.5}$  collected in a magnetic field  $\mu_0 H=30$  mT at temperatures above ( $T=20$  K) and below ( $T=1.2$  K) the superconducting transition temperature  $T_c=14.4$  K.

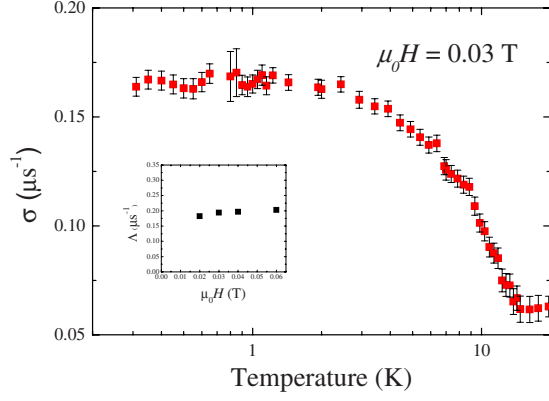


FIG. 4. (Color online) The temperature dependence of the Gaussian depolarization rate  $\sigma$  extracted from the TF muon-time spectra collected in an applied magnetic field  $\mu_0 H = 30$  mT. The inset demonstrates the magnetic field independence of the parameter  $\Lambda$  at 20 K.

$+\sigma_{nm}^2)^{1/2}$ .  $\sigma_{sc}(T)$  is the contribution to the relaxation arising from the vortex lattice while  $\sigma_{nm}$ , the nuclear magnetic dipolar term, is assumed to be temperature independent over the temperature range of the measurements. The data were fitted in two steps. First the data in the two channels were fitted simultaneously at each temperature with  $A_0$ ,  $\Lambda$ , and  $\sigma$  as common variables. The fits were checked over the entire temperature range to ensure that physical values were obtained for all the parameters at each temperature point. To ensure stability of the fits  $\Lambda$  was then fixed to the value obtained just above  $T_c$  and the data were refitted at each temperature point. The temperature dependence of  $\sigma$  obtained is shown in Fig. 4.

In a superconductor with a large upper critical field and a hexagonal Abrikosov vortex lattice, the Gaussian muon-spin depolarization rate,  $\sigma_{sc}(T)$ , is related to the penetration depth  $\lambda$  by the expression

$$\frac{2\sigma_{sc}^2(T)}{\gamma_\mu^2} = 0.00371 \frac{\Phi_0^2}{\lambda^4(T)}, \quad (5)$$

where  $\gamma_\mu/2\pi = 135.5$  MHz/T is the muon gyromagnetic ratio and  $\Phi_0 = 2.068 \times 10^{-15}$  Wb is the flux quantum.<sup>11,12</sup> The temperature dependence of the penetration depth can then be fitted using either a single-gap or a two-gap model,<sup>16,17</sup>

$$\frac{\lambda^{-2}(T)}{\lambda^{-2}(0)} = \omega_1 \frac{\lambda^{-2}(T, \Delta_{0,1})}{\lambda^{-2}(0, \Delta_{0,1})} + \omega_2 \frac{\lambda^{-2}(T, \Delta_{0,2})}{\lambda^{-2}(0, \Delta_{0,2})}, \quad (6)$$

where  $\lambda^{-2}(0)$  is the value of the penetration depth at  $T = 0$  K,  $\Delta_{0,i}$  is the value of the  $i$ th ( $i = 1$  or  $2$ ) superconducting gap at  $T = 0$  K and  $\omega_i$  is the weighting factor with  $\omega_1 + \omega_2 = 1$ .

Each term in Eq. (6) is evaluated using the standard expression within the local London approximation<sup>18,19</sup>

TABLE I. Results for fits to the temperature dependence of the penetration depth using different models for the symmetry of the superconducting gap function (Ref. 20).

Model	$g(\varphi)$	Gap value (meV)	$\chi^2$
$s$ wave	1	$\Delta = 1.86(2)$	5.93
$s+s$ wave	1	$\Delta_1 = 2.6(1)$ , $\Delta_2 = 0.87(6)$ , and $\omega_1 = 0.70(3)$	1.55
Anisotropic			
$s$ wave	$(s + \cos 4\varphi)$	$\Delta = 1.4(1)$ with $s = 1.56(5)$	1.62
$d$ wave	$ \cos(2\varphi) $	$\Delta = 3.31(4)$	2.87

$$\frac{\lambda^{-2}(T, \Delta_{0,i})}{\lambda^{-2}(0, \Delta_{0,i})} = 1 + \frac{1}{\pi} \int_0^{2\pi} \int_{\Delta(T, \varphi)}^{\infty} \left( \frac{\partial f}{\partial E} \right) \frac{E dE d\varphi}{\sqrt{E^2 - \Delta_i(T, \varphi)^2}}, \quad (7)$$

where  $f = [1 + \exp(E/k_B T)]^{-1}$  is the Fermi function,  $\varphi$  is the angle along the Fermi surface, and  $\Delta_i(T, \varphi) = \Delta_{0,i} \delta(T/T_c) g(\varphi)$ . The temperature dependence of the gap is approximated by the expression  $\delta(T/T_c) = \tanh\{1.82[1.018(T_c/T - 1)]^{0.51}\}$  (Ref. 16) while  $g(\varphi)$  describes the angular dependence of the gap. The fits (see Table I) appear to rule out both the  $d$  wave and  $s$  wave as possible models for this system.<sup>20</sup>

The anisotropic  $s$ -wave model gives a value for  $s$ , the parameter reflecting the isotropic  $s$ -wave component, that is larger than that obtained for FeSe<sub>0.85</sub> in Ref. 15. Nevertheless, the variation in the gap with angle  $\Delta_{max}/\Delta_{min} \approx 4.6$  is still larger than the published values for related single layer superconductor NdFeAsO<sub>0.9</sub>F<sub>0.1</sub>.<sup>21</sup>

A fit to the data using a two-gap  $s+s$ -wave model is shown in Fig. 5 and gives  $\Delta_{0,1} = 2.6(1)$  meV and  $\Delta_{0,2} = 0.87(6)$  meV with  $\omega_1 = 0.70(3)$ . This model gives the lowest  $\chi^2$ .  $\omega_1$  agrees with the value obtained by  $\mu$ SR for FeSe<sub>0.85</sub>, where  $\omega_1 = 0.658(3)$ .<sup>15</sup> The size of the larger energy gap for FeSe<sub>0.85</sub> and FeTe<sub>0.5</sub>Se<sub>0.5</sub> scale with  $T_c$ . The ratio  $\Delta_{0,1}/\Delta_{0,2} \sim 3$  found in FeTe<sub>0.5</sub>Se<sub>0.5</sub> is 40% smaller than the

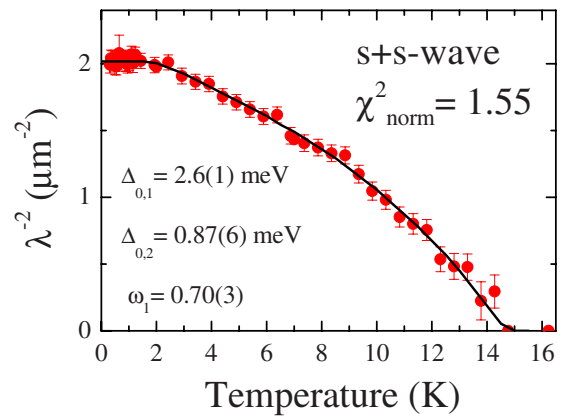


FIG. 5. (Color online) Temperature dependence of  $\lambda^{-2}$  for FeTe<sub>0.5</sub>Se<sub>0.5</sub>. The curve (black line) is a fit to the data using two  $s$ -wave components, each with an isotropic gap.

corresponding value seen in  $\text{FeSe}_{0.85}$  but coincides with the value for  $R\text{FeAsO}_{0.9}\text{F}_{0.1}$  ( $R=\text{La, Nd}$ ) determined by measuring the magnetic penetration depth using a tunnel-diode resonator.<sup>22</sup>

For anisotropic polycrystalline samples, the magnetic penetration depth,  $\lambda$ , calculated from the  $\mu\text{SR}$  depolarization rate  $\sigma$  is related to  $\lambda_{ab}$ , the in-plane penetration depth by  $\lambda = 3^{1/4}\lambda_{ab}$ .<sup>23,24</sup> At  $T=0$ , the value for  $\lambda(0)=703(2)$  nm with  $\lambda_{ab}(0)=534(2)$  nm.<sup>25</sup> These values are longer than those obtained by Khasanov *et al.*<sup>15</sup> for  $\text{FeSe}_{0.85}$  in spite of the fact that the  $T_c$  of  $\text{FeTe}_{0.5}\text{Se}_{0.5}$  is  $\sim 6$  K higher. The value for  $\lambda$  would place  $\text{FeTe}_{0.5}\text{Se}_{0.5}$  above the line for hole doped high  $T_c$  cuprates on an Uemura plot.<sup>26,27</sup>

Using an upper critical field,  $B_{c2}(0)\parallel ab$ , for  $\text{FeTe}_{0.5}\text{Se}_{0.5}$  estimated from transport and magnetization measurements of 50 T and  $B_{c2}=\frac{\Phi_0}{2\pi\xi^2}$ , we calculate a coherence length,  $\xi_{ab}$ , for  $\text{FeTe}_{0.5}\text{Se}_{0.5}$  at 0 K of  $\sim 2.6$  nm. If this is combined with our measurement of  $\lambda$  and the standard expression  $H_{c1}=\frac{\Phi_0}{4\pi\lambda^2}(\ln\frac{\lambda}{\xi}+0.12)$  (Ref. 18) we estimate  $\mu_0H_{c1}(0)\parallel ab=3.2$  mT. This is in fair agreement with magnetization measurements where the first deviation from linear behavior

gives  $\mu_0H_{c1}\parallel ab$  of between 1 and 8 mT at 1.5 K.<sup>9,10</sup>

In summary,  $\mu\text{SR}$  measurements have been performed on superconducting  $\text{FeTe}_{0.5}\text{Se}_{0.5}$ . The temperature dependence of the magnetic penetration depth is found to be compatible with either a two-gap  $s+s$ -wave or an anisotropic  $s$ -wave model. This result is consistent with other experimental data<sup>15,28</sup> and density-functional calculations of the physical properties<sup>29</sup> of the  $\text{FeTe}_{1-x}\text{Se}_x$  system, and with the more general picture that is now emerging for iron pnictide superconductors in which they are described as two-band superconductors. Further studies on high-purity single-crystal samples are desirable as the presence of impurities can sometimes mask the true nature of the superconducting gap.<sup>30</sup>

The Quantum Design MPMS magnetometer used in this research was obtained through the Science City Advanced Materials project: Creating and Characterizing Next Generation Advanced Materials Project, with support from Advantage West Midlands (AWM) and partially funded by the European Regional Development Fund (ERDF).

\*Also at Department of Physics, Indian Institute of Technology, Bombay, Mumbai 40076, India.

†m.r.lees@warwick.ac.uk

<sup>1</sup>Y. Kamihara, T. Watanabe, M. Hirano, and H. Hosono, *J. Am. Chem. Soc.* **130**, 3296 (2008).

<sup>2</sup>H. Takahashi, K. Igawa, K. Arii, Y. Kamihara, M. Hirano, and H. Hosono, *Nature (London)* **453**, 376 (2008).

<sup>3</sup>X. H. Chen, T. Wu, G. Wu, R. H. Liu, H. Chen, and D. F. Fang, *Nature (London)* **453**, 761 (2008).

<sup>4</sup>F.-C. Hsu *et al.*, *Proc. Natl. Acad. Sci. U.S.A.* **105**, 14262 (2008).

<sup>5</sup>S. Margadonna, Y. Takabayashi, Y. Ohishi, Y. Mizuguchi, Y. Takano, T. Kagayama, T. Nakagawa, M. Takata, and K. Prasad, *Phys. Rev. B* **80**, 064506 (2009).

<sup>6</sup>K.-W. Yeh *et al.*, *Europhys Lett.* **84**, 37002 (2008).

<sup>7</sup>M. H. Fang, H. M. Pham, B. Qian, T. J. Liu, E. K. Vehstedt, Y. Liu, L. Spinu, and Z. Q. Mao, *Phys. Rev. B* **78**, 224503 (2008).

<sup>8</sup>T. Kida, T. Matsunaga, M. Hagiwara, Y. Mizuguchi, Y. Takano, and K. Kindo, *J. Phys. Soc. Jpn.* **78**, 113701 (2009).

<sup>9</sup>C. S. Yadav and P. L. Paulose, *New J. Phys.* **11**, 103046 (2009).

<sup>10</sup>P. K. Biswas, G. Balakrishnan, C. V. Tomy, D. M. Paul, and M. R. Lees (unpublished).

<sup>11</sup>J. E. Sonier, J. H. Brewer, and R. F. Kiefl, *Rev. Mod. Phys.* **72**, 769 (2000).

<sup>12</sup>E. H. Brandt, *Phys. Rev. B* **37**, 2349 (1988).

<sup>13</sup>F. Walz, *J. Phys.: Condens. Matter* **14**, R285 (2002).

<sup>14</sup>The magnetization at 5 and 20 K is  $\sim 30$  times smaller than that reported in the sample of  $\text{FeSe}_{0.85}$  studied by Khasanov *et al.* (Ref. 15).

<sup>15</sup>R. Khasanov, K. Conder, E. Pomjakushina, A. Amato, C. Baines, Z. Bukowski, J. Karpinski, S. Katrych, H.-H. Klauss, H. Luetkens, A. Shengelaya, and N. D. Zhigadlo, *Phys. Rev. B* **78**, 220510(R) (2008).

<sup>16</sup>A. Carrington and F. Manzano, *Physica C* **385**, 205 (2003).

<sup>17</sup>H. Padamsee, J. E. Neighbor, and C. A. Shiffman, *J. Low Temp. Phys.* **12**, 387 (1973).

<sup>18</sup>M. Tinkham, *Introduction to Superconductivity* (McGraw-Hill, New York, 1975).

<sup>19</sup>R. Prozorov and R. W. Giannetta, *Supercond. Sci. Technol.* **19**, R41 (2006).

<sup>20</sup>The normalized  $\chi^2$  values, resulting from our least-squares fits to the temperature dependence of  $\lambda^{-2}$  using different models for the gap, are used as criteria to determine which model best describes the data.

<sup>21</sup>T. Kondo *et al.*, *Phys. Rev. Lett.* **101**, 147003 (2008).

<sup>22</sup>C. Martin *et al.*, *Phys. Rev. Lett.* **102**, 247002 (2009).

<sup>23</sup> $\mu\text{SR}$  cannot measure  $\lambda$  along a single crystallographic direction. The measurements are limited to mixed quantities, which here is  $\lambda_{ab}=(\lambda_a\lambda_b)^{1/2}$ .

<sup>24</sup>V. Fesenko, V. Gorbunov, and V. Smilga, *Physica C* **176**, 551 (1991).

<sup>25</sup>The error in  $\lambda(0)$  is the statistical error arising from the fit to the  $\lambda^{-2}(T)$  data using the model described in the text. The error quoted does not take into account any systematic errors (e.g., vortex lattice disorder) that may be present in the data.

<sup>26</sup>Y. J. Uemura *et al.*, *Phys. Rev. Lett.* **62**, 2317 (1989).

<sup>27</sup>H. Luetkens *et al.*, *Phys. Rev. Lett.* **101**, 097009 (2008).

<sup>28</sup>J. K. Dong, T. Y. Guan, S. Y. Zhou, X. Qiu, L. Ding, C. Zhang, U. Patel, Z. L. Xiao, and S. Y. Li, *Phys. Rev. B* **80**, 024518 (2009).

<sup>29</sup>A. Subedi, L. Zhang, D. J. Singh, and M. H. Du, *Phys. Rev. B* **78**, 134514 (2008).

<sup>30</sup>J. E. Sonier, J. H. Brewer, R. F. Kiefl, G. D. Morris, R. I. Miller, D. A. Bonn, J. Chakhalian, R. H. Heffner, W. N. Hardy, and R. Liang, *Phys. Rev. Lett.* **83**, 4156 (1999), and references therein.